A Design Approach for Robustness Improvement of Rate Gyroscopes

Cenk Acar* and Andrei Shkel**

Microsystems Laboratory, Department of Mechanical and Aerospace Engineering
University of California, Irvine, CA, USA
*cacar@uci.edu, **ashkel@uci.edu, http://mems.eng.uci.edu

ABSTRACT

This paper reports a design concept for robustness improvement of micromachined gyroscopes. The novelty of the approach is in expanding the design space of the device by increasing the degrees-of-freedom (DOF) of the system. The approach facilitates the use of two independently oscillating proof masses instead of one as is done in classical designs. Utilization of the dynamic amplification approach in the 4 DOF system eliminates the necessity of operating the device in the resonance mode. Simulations indicate over 15 times increase in the bandwidth of the system, which demonstrates a significantly improved robustness against structural and thermal parameter fluctuations over the operating time of the device.

Keywords: MEMS, inertial sensors, micromachined gyroscopes.

1 INTRODUCTION

All existing micromachined rate gyroscopes operate on the vibratory principle of a single proof mass suspended by flexures anchored to the substrate. The flexures serve as the flexible suspension between the proof mass and the substrate, allowing the mass to oscillate freely in two orthogonal directions - the drive and the sense [1]. The proof mass is driven into resonance in the drive direction by an external sinusoidal force with a certain drive frequency. If the gyroscope is subjected to an angular rotation, the Coriolis force is induced in the y-direction. The resulting oscillation amplitude in the sense direction is proportional to the Coriolis force, and thus to the angular velocity to be measured [2].

To achieve the maximum possible gain, conventional gyroscopes are designed to operate at the peak of the response curve. This is typically achieved by matching drive and sense resonant frequencies (Fig. 2). However, the system is very sensitive to variations in system parameters causing a shift in the resonant frequencies. For example, a 1% fluctuation in frequency matching between drive and sense modes will produce an error of 20% in the output signal gain [3]. Under high quality factor conditions, the gain is high, but the bandwidth is extremely narrow. Furthermore, the gain is affected significantly by fluctuations in damping (Fig. 2).

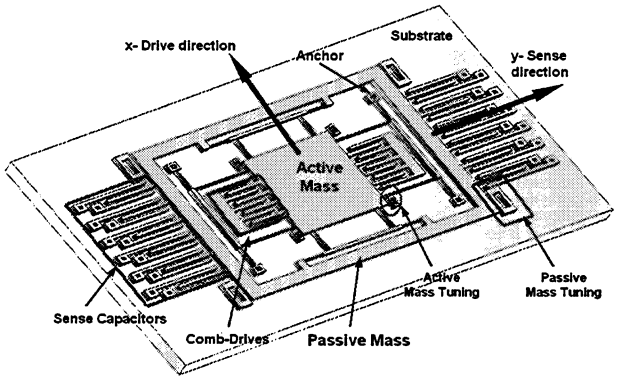

Figure 1: Illustration of the dual-mass z-axis gyroscope.

Fabrication imperfections are inevitable, and affect material properties and geometry of MEMS structures. Thus, changes in elastic modulus, beam thickness and residual stresses have significant effects on the resonant frequencies of gyroscopes. Generally, sophisticated control electronics is required to maintain operation in the region of the resonance peak [4]. To eliminate the limitations of the existing micromachined gyroscopes, a design approach that facilitates the use of two oscillating proof masses (Fig. 1) is proposed.

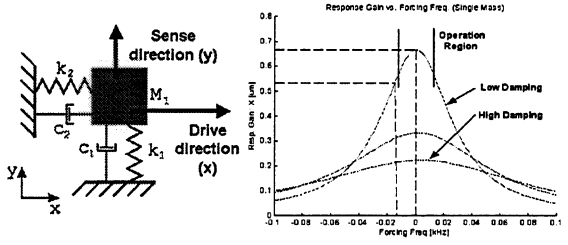

Figure 2: Schematic of a conventional gyroscope, which has two principle directions: drive and sense. The gain is very sensitive to drive and sense mode resonant frequency, matching variations, and damping fluctuations.

2 PRINCIPLE OF OPERATION

In contrast to conventional micromachined gyroscopes, the proposed approach utilizes dynamic amplification of mechanical motion without requiring the system to operate in resonance [5]. In order to achieve dynamic amplification, a system containing two independently vibrating proof masses (Fig. 3 is used). In the system, the first mass is forced to oscillate in the drive direction. This forced oscillation is amplified by the second mass. The response of this passive mass to the rotation induced Coriolis force is monitored providing the angular rate of object rotation.

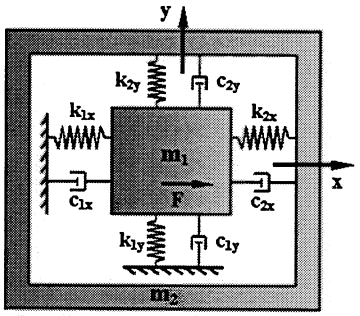

Figure 3: Schematic of a lumped model of the dual-mass gyroscope. The first mass is driven in the x direction, and the response of the second mass along the y-axis is sensed.

With appropriate selection of system parameters, one can obtain a frequency response illustrated in Fig. 4. There exist three regions of interest on this response curve: two resonant peaks (regions 1 and 3) and a flat region between the peaks (region 2). The nominal operation of the gyroscope is in the flat region, where the signal gain is relatively high, and the sensitivity of the gain to driving frequency variations is low [3].

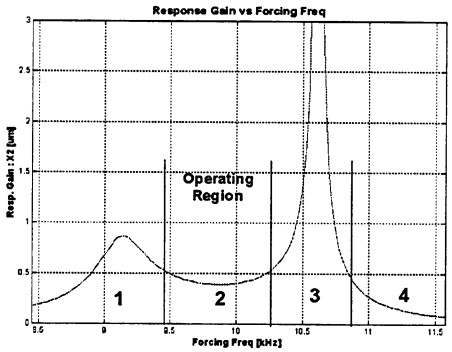

Figure 4: Response of the dual-mass gyroscope includes two resonant peaks (regions 1 and 3) and a flat region between the peaks (region 2), which is the nominal operation region.

To achieve the maximum possible response of the gyroscope, amplitude of the drive-direction oscillation of the passive mass should be maximized. When the driving frequency is matched with the resonant frequency of the isolated passive mass-spring system - maximum dynamic amplification is achieved.

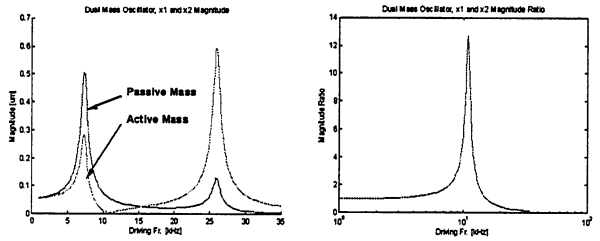

Figure 5: (a) The drive-mode magnitudes of each mass. At the antiresonant frequency, oscillation amplitude of the controlled mass approaches to zero. (b) The dynamic amplification ratio reaches its maximum at the resonant frequency of the isolated passive mass-spring system.

3 DESIGN APPROACH AND IMPLEMENTATION

An implementation of the conceptual design, Fig. 3, is illustrated in Fig. 6 (also see [5]). The dynamic system of the proposed micromachined gyroscope consists of two vibrating proof masses, flexures between the active mass and the ground which are anchored to the substrate, and flexures between the active mass and the passive mass, mechanically coupling the masses (Fig. 6).

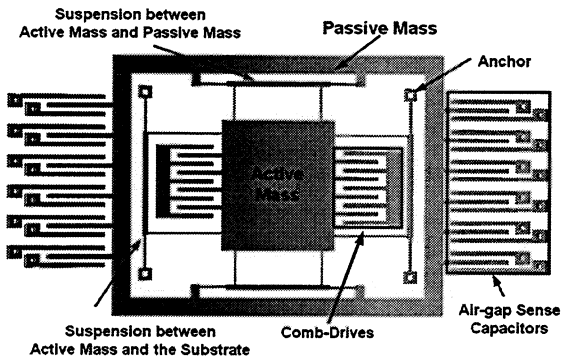

Figure 6: Simplified illustration of the dual-mass z-axis gyroscope.

The complete suspension system consists of two sets of four flexible beams per each mass (Fig. 6). One set of fixed-guided beams provides the desired spring rate in the drive direction, while the other set provides the desired spring rate in the sense direction [5].

Spring rates for a mass in drive or sense direction are determined by translational stiffness of four fixed-guided beams if the axial strains in the other beams

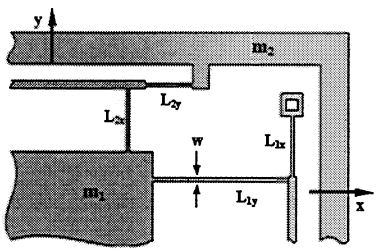

Figure 7: The proposed configuration of the suspension allows proof masses to freely oscillate within a plane of operation.

are neglected. Thus, each stiffness value in the dynamic system can be calculated as [6]:

$$k_{1x} = \frac{4Etw^3}{L_{1x}^3}\ ,\ k_{1y} = \frac{4Etw^3}{L_{1y}^3}\ ,\ k_{2x} = \frac{4Etw^3}{L_{2x}^3}\ ,\ k_{2y} = \frac{4Etw^3}{L_{2y}^3}$$

where E is the Young's Modulus, w is the width of the beam elements in the suspension, and t is the thickness of the structure. The individual beam lengths are shown in Fig. 7.

The damping values in the dynamic system can be represented as a combination of Couette flow between the masses and the substrate, Couette flow or squeeze film damping between the integrated comb fingers or the air gap capacitors [2]

$$c_{1x} = \mu_p p\frac{A_1}{z_0} + \mu_p p\frac{2N_{comb}l_{comb}t}{y_{comb}},$$

$$c_{1y} = \mu_p p\frac{A_1}{z_0} + \mu_p p\frac{7N_{comb}l_{comb}t^3}{y_{comb}^3},$$

$$c_{2x} = \mu_p p\frac{A_2}{z_0} + \mu_p p\frac{2N_{cap}l_{cap}t}{y_{cap}},$$

$$c_{2y} = \mu_p p\frac{A_2}{z_0} + \mu_p p\frac{7N_{cap}l_{cap}t^3}{y_{cap}^3}.$$

Here, A_1 and A_2 are the areas of the active and passive masses respectively; z_0 is the elevation of the proof mass from the substrate; t is the thickness of the suspension; N_{comb}, N_{cap}, l_{comb}, and l_{cap} are the number and length of comb-drive electrodes and air-gap capacitors, respectively. y_{comb} and y_{cap} are the distances between the fingers, p is the ambient pressure within the cavity of the packaged device, and $\mu_p = 3.710^{-4}\frac{kg}{m^2 storr}$ is the viscosity constant for air.

In the drive mode, a sinusoidal force $F = F_0 sin(\omega t)$ is applied to the active mass by the comb-drive structure that imposes a balanced interdigitated comb-drive scheme. Applying $V_1 = V_{DC} + \nu_{AC}$ to one set of comb drives (e.g. the set on the right side in Fig. 6), and $V_2 = V_{DC} - \nu_{AC}$ to the opposing set (the set on the left side), the net electrostatic force is linear to ν_{AC}, which will lead to simplification of the dynamic model

$$F = 4\frac{\varepsilon_0 z_0 N}{y_0} V_{DC}\nu_{AC}$$

Here, $\nu_{AC} = |\nu_{AC}|sin(\omega t)$ is the sinusoidal voltage, V_{DC} is the constant bias voltage, z_0 is the finger thickness, and y_0 is the finger separation.

4 DYNAMICS OF THE GYROSCOPE

When the active and passive masses are observed in the non-inertial rotating frame, the "gyroscope frame", additional inertial forces appear acting on both masses [4]. The equations of motion for the two-mass system can be written as

$$m_1\vec{a_1} = \vec{F_{2-1}} + \vec{F_{s-1}} - 2m_1\vec{\Omega}\mathrm{x}\vec{v_1} - m_1\vec{\Omega}\mathrm{x}(\vec{\Omega}\mathrm{x}\vec{r_1}) - m_1\dot{\vec{\Omega}}\mathrm{x}\vec{r_1}$$
$$m_2\vec{a_2} = \vec{F_{1-2}} + \vec{F_{s-2}} - 2m_2\vec{\Omega}\mathrm{x}\vec{v_2} - m_2\vec{\Omega}\mathrm{x}(\vec{\Omega}\mathrm{x}\vec{r_2}) - m_2\dot{\vec{\Omega}}\mathrm{x}\vec{r_2}$$

where $\vec{r_1}$ and $\vec{r_2}$ are the position vectors, and $\vec{v_1}$ and $\vec{v_2}$ are the velocity vectors of the masses defined in the gyroscope frame. $\vec{F_{2-1}}$ and $\vec{F_{1-2}}$ are the opposing coupling forces between the masses that each mass applies on the other depending on relative position $\vec{r_2} - \vec{r_1}$, including spring and damping forces. $\vec{F_{s-1}}$ consists of spring and damping forces between the active mass and the substrate and $\vec{F_{s-2}}$ includes the passive mass - substrate damping force. Since both masses are subjected to an angular rate of Ω about the axis normal to the plane of operation (z-axis), the equations of motion along the x-axis and y-axis become

$$m_1\ddot{x_1} + c_{1x}\dot{x_1} + k_{1x}x_1 = k_{2x}(x_2 - x_1) + c_{2x}(\dot{x_2} - \dot{x_1}) + m_1\Omega^2 x_1 - 2m_1\Omega\dot{y_1} + m_1\dot{\Omega}y_1 + F_d(t)$$

$$m_2\ddot{x_2} + c_{2x}(\dot{x_2} - \dot{x_1}) + k_{2x}(x_2 - x_1) = m_2\Omega^2 x_2 - 2m_2\Omega\dot{y_2} + m_2\dot{\Omega}y_2$$

$$m_1\ddot{y_1} + c_{1y}\dot{y_1} + k_{1y}y_1 = k_{2y}(y_2 - y_1) + c_{2y}(\dot{y_2} - \dot{y_1}) + m_1\Omega^2 y_1 - 2m_1\Omega\dot{x_1} + m_1\dot{\Omega}x_1$$

$$m_2\ddot{y_2} + c_{2y}(\dot{y_2} - \dot{y_1}) + k_{2y}(y_2 - y_1) = m_2\Omega^2 y_2 - 2m_2\Omega\dot{x_2} + m_2\dot{\Omega}x_2.$$

Here, $F_d(t)$ is the driving electrostatic force applied to the active mass and Ω is the angular velocity applied to the gyroscope about the z-axis.

The overall dynamic model can be reduced by driving the active mass in the drive direction by $F_d(t)$ with a constant amplitude x_o and a frequency ω_d. Assuming the oscillation of the first mass in the drive direction is set by the control system to be

$$x_1 = x_o cos(\omega_d t),$$

the system reduces to 3 degrees of freedom. The equations of motion of the system become [3]

$$\ddot{y_1} + 2\omega_n\xi\dot{y_1} + 2\mu\omega_n\xi(\dot{y_1} - \dot{y_2}) + (\omega_n - \Omega)y_1 + \omega_n^2\sigma_1(y_1 - y_2) = -2\Omega\omega_d x_o sin\omega_d t + \dot{\Omega}x_o cos\omega_d t$$

$$\beta(\ddot{y_2} - \Omega^2 y_2) + 2\mu\omega_n\xi(\dot{y_2} - \dot{y_1}) - 2\beta\Omega\dot{x_2} - \beta\dot{\omega_z}x_2 + \omega_n^2\sigma_1(y_2 - y_1) = 0$$

$$\beta(\ddot{x_2} - \Omega^2 x_2) + 2\beta\Omega\dot{y_2} + \beta\dot{\Omega}y_2 + \omega_n^2\sigma_2 x_2 = w_n^2\sigma_2 x_o cos\omega_d t$$

where $\beta = m_2/m_1$, $\sigma_1 = k_{2y}/k_{1y}$, $\sigma_2 = k_{2x}/k_{1x}$, $\mu = c_2/c_1$, $\xi = c_1/(2m_1w_n)$, and w_n is the natural frequency in the sense direction .

5 MODELING RESULTS

Sensitivity analysis of the proposed design is studied in this section. Fabrication variations can affect the parameters of gyroscopes directly. The thickness of the gyroscope structure is determined by deposition processes, and the width of the suspension beam elements set by lithography is affected by etching processes. In conventional gyroscopes, fabrication variations result in resonant frequency shifts, requiring compensation by sophisticated control electronics. For the proposed system, a 0.05 μm deviation from 2 μm nominal beam width or a 0.1 μm deviation from 2 μm nominal structure thickness results in less than 1% error in the gain (Fig. 8b and c). Moreover, a variation in deposition conditions that affect the Young's Modulus of the gyroscopes structure by 10 MPa causes less than 0.5 % error (Fig. 8d). The same parameter variations in a conventional micromachined gyroscope without compensation by control system can result in over 10% error.

Pressure fluctuations can have significant effects on conventional gyroscopes (Fig. 2). However, since the proposed device does not operate in resonance, the response is insensitive to damping changes in the operation region (Fig. 9). For a possible vacuum leakage due to package sealing defects over the operation time of the device from 100 militorrs to 500 militorrs, the device gain reduces by less than 2% (Fig. 8a), where the same pressure variation can result in over 20% gain reduction in a conventional gyroscope design.

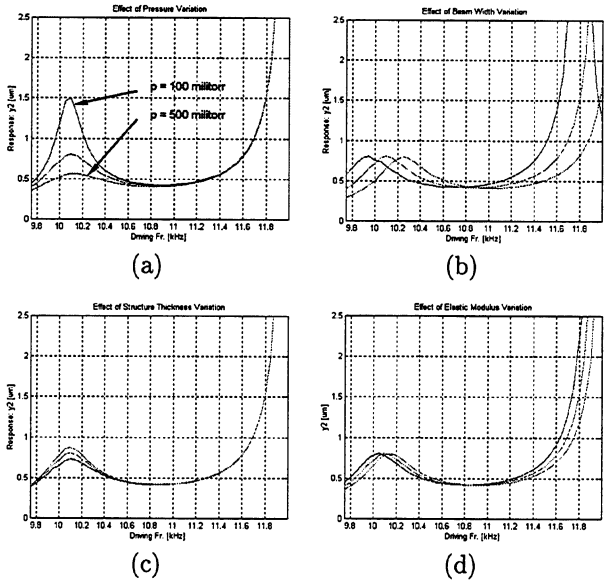

Figure 8: Effect of (a) ambient pressure change form 100 militorrs to 500 militorrs, (b)0.05μm variation in the width of suspension beams, (c)0.1μm variation in structure thickness, (d)10 MPa variation in Young's Modulus, on the response.

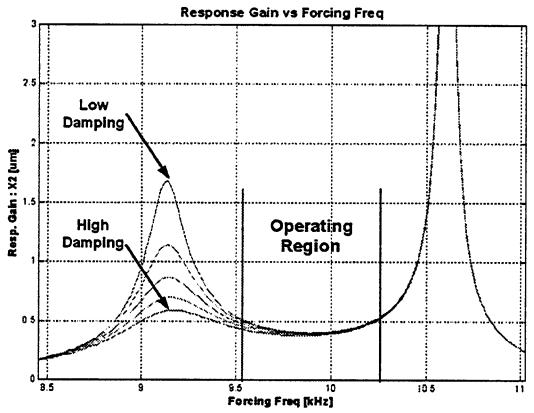

Figure 9: The response in the operation region is insensitive to variations in damping, which can, e.g. relax packaging requirements.

6 CONCLUSION

A new design approach for increasing robustness of MEMS gyroscopes is presented, the design and the dynamical system are analyzed, and effects of realistic parameter variations on the system response are investigated. The implementation of the idea is based on the use of two independently oscillating proof masses. By utilizing dynamical amplification, the necessity of operation in the resonance mode is eliminated, and over 15 times increase in the bandwidth of the system is achieved. The proposed device is demonstrated to have improved robustness against expected fabrication and packaging fluctuations, especially against damping variations due to ambient pressure, compared to the conventional gyroscopes. Consequently, tight fabrication tolerances and packaging requirements can be relaxed, resulting in a lower production cost of MEMS gyroscopes.

REFERENCES

[1] N. Yazdi, F. Ayazi, and K. Najafi. Micromachined Inertial Sensors. *Proc. of IEEE, Vol. 86, No. 8*, August 1998.

[2] W.A. Clark, R.T. Howe, and R. Horowitz. Surface Micromachined Z-Axis Vibratory Rate Gyroscope. *Proc. of Solid-State Sensor and Actuator Wsp.*, June 1994.

[3] E. Netzer, and I. Porat. A Novel Vibratory Device for Angular Rate Measurement. *J.of Dynamic Systems, Measurement and Control*, Dec. 1995.

[4] A. Shkel, R. Horowitz, A. Seshia, S. Park and R.T. Howe. Dynamics and Control of Micromachined Gyroscopes *American Control Conf., CA* ,1999.

[5] C. Acar and A. Shkel. Wide Bandwidth Micromachined Gyroscope to Measure Rotation. *Patent pending, UCI O.T.A.*, Case No:2001-140-1.

[6] W.C. Young. Roark's Formulas for Stress & Strain. *McGraw-Hill, Inc.*, 93-156, 1989.